Calculations of a Turbulent Bluff-Body Stabilized Flame

K. Liu[*], S. B. Pope and D. A. Caughey
Sibley School of Mechanical and Aerospace Engineering
Cornell University, Ithaca, NY 14853

Abstract
The Joint velocity-turbulent frequency-composition Probability Density Function (JPDF) method implemented in a hybrid Finite Volume (FV)/particle algorithm is applied to a bluff-body stabilized flame. The *in situ* adaptive tabulation (ISAT) method is used to implement methane chemistry using an Augmented Reduced Mechanism (ARM). Numerically accurate results are obtained. Comparisons with experimental data are shown for: profiles of the mean and r.m.s. of mixture fraction; profiles of temperature and mean species mass fractions; and scatter plots of species mass fraction against mixture fraction. The JPDF calculations are in reasonable agreement with the experimental data.

Introduction

The interaction between turbulent mixing and finite-rate chemical reaction is the most important issue in turbulence combustion. Bluff-body stabilized flames provide an ideal case for testing models for these interactions. There is a complex recirculation zone which stabilizes the flame, and which results in complicated interactions between the turbulence and finite-rate chemical reactions. At the same time, the boundary conditions are quite simple.

Masri *et al.* [1] have conducted comprehensive experimental investigations on a series of bluff-body flames, including flames from fully burning to those exhibiting local extinction. All the experimental data are available online [1]. Using the above data as a benchmark, many researchers have contributed to the understanding and modeling of these flames. Dally *et al* [2] investigated the performance of k-ε and Reynolds Stress Models (RSM) on the bluff-body flames using a flamelet model. Merci *et al.* [3] have investigated the performance of a new cubic nonlinear k-ε model using a simplified constrained equilibrium model. Hossain, *et al* [4] also used the k-ε model with a flamelet model to investigate the effects of heat radiation. Kim *et al.* [5] applied the first order Conditional Moment Closure (CMC) modeling using GRI chemistry to the bluff-body flames to predict NO formation. In all the above modeling methodologies, the treatment of chemical reaction is based on mixture fraction. Present day mixture fraction based models cannot predict local extinction and reignition behavior.

The joint velocity-turbulence frequency-composition PDF (JPDF) method has been demonstrated to be a successful modeling approach for turbulent combustion [6, 7]. A primary advantage of this approach is that the chemical reaction terms are in closed form in the JPDF transport equation and can be treated in exact form. Chemical reaction calculations are implemented by *in situ* adaptive tabulation (ISAT) [8], which can improve the efficiency of chemistry calculations by several orders of magnitude. Meanwhile, a recently-developed, fully-consistent, hybrid finite volume/Monte Carlo particle algorithm dramatically improves the numerical efficiency of the JPDF method [9]. These advances make it possible to perform detailed chemistry calculations for a complicated flame such as the bluff-body stabilized flame.

Muradoglu *et al.* [10] have applied JPDF modeling to a bluff-body flame using a simple flamelet model to investigate the sensitivity of the calculations to boundary conditions and model constants. At TNF6, Liu *et al.* [11] have shown results for this flame using a relatively simple skeletal chemical mechanism. Since the augmented reduced mechanism for methane (ARM) [12] has been successfully used in previous piloted jet flame calculations [7], it is also expected to be successful for bluff-body flames.

Specific Objectives

The purpose of this paper is to describe recent calculations using the JPDF method combined with a fully-consistent hybrid FV/particle algorithm with realistic chemistry implemented using ISAT. The Sydney bluff-body flame HM1 [1] is chosen as the target flame for the present JPDF calculations. First, with a simple flamelet chemistry model, grid refinement tests are performed to demonstrate the grid convergence of the calculations. Then calculations using ARM are performed, and the results are compared with the experimental data. We also investigate the sensitivity of the calculated results to the value of the model constant C_ϕ used in the interaction by exchange with the mean (IEM) mixing model.

---

[*] Corresponding author: kl47@cornell.edu

The Flame Specifications

Hydrogen-Methane (HM) flames comprise one set of the Sydney bluff-body flames [1]. They include HM1, HM2 and HM3, which are distinguished by having different jet bulk velocities. HM1 is selected as the target flame of the current work. HM2 and HM3, which have larger jet bulk velocities and consequently higher degrees of local extinction and reignition, will be studied in the future.

The experimental configuration and specifications of HM1 are briefly summarized here. The burner consists of a fuel jet surrounded by a bluff-body and co-flowing air. The diameter of jet, D_J, is 3.6mm and the diameter of bluff-body, D_B, is 50mm. The jet fuel is a mixture of methane, CH_4, and hydrogen, H_2, 1:1 by volume, with the bulk velocity, $U_J = 118$m/s. The co-flow velocity is $U_C = 40$m/s.

There is a recirculation zone immediately downstream of the bluff-body surface which extends to about 1.6 D_B and stabilizes the flame. Downstream of the recirculation zone is the neck zone from about 1.6 D_B to about 2.4 D_B. Further downstream there is a jet-like zone. The effects of the interaction between turbulent mixing and finite-rate chemical reactions are very important within the neck zone.

JPDF methodology and modeling

The hybrid FV/particle algorithm has been developed by Muradoglu *et al.* [9], based on the previous stand-alone Joint PDF method. In the hybrid algorithm, the joint fluctuation velocity-turbulence frequency-composition PDF transport equation is solved by a particle-in-cell Monte Carlo method (called the particle part), and the mean conservation equations of density, momentum, and energy, directly derived from the PDF transport equation, are solved by a finite volume (FV) solver (called the FV part). The two parts are coupled as follows: the FV part provides mean fields of velocity, density and pressure to the particle part and obtains the turbulent fluxes and reaction source term from the particle part. Although the algorithm is fully consistent at the differential equation level, correction algorithms are necessary to guarantee consistency of the duplicate fields at the numerical level [9].

The hybrid algorithm dramatically reduces the bias errors compared with the previous stand-alone particle method [13]. The computational efficiency is thereby improved by allowing the use of fewer particles per cell, N_{PC} for a given level of error. Also, the implementation of local variable time-stepping accelerates the global convergence process [14].

The ingredients of the JPDF model include: the simplified Langevin model (SLM) [3] employed for velocity, the Jayesh-Pope model (JPM) [15] for turbulence frequency, and the Interaction by Exchange with Mean (IEM) model [16] for turbulent mixing. The model constants used are the same as those in [11] and are listed in Table 1 for completeness.

The ARM mechanism used here includes 19 species and 15 reactions. C_2 species and three NO related species and their reactions are included [12]. This mechanism is denoted as ARM2 to distinguish it from a previous ARM mechanism, which does not include NO related species and reactions.

Table 1: Model Constants

Constant:	Standard Value:	Model:
C_0	2.1	SLM
C_Ω	0.6893	Definition of Ω
$C_{\omega 1}$ $C_{\omega 2}$ C_3 C_4	0.65 0.9 1.0 0.25	JPM
C_ϕ	2.0	IEM

Numerical parameters and solutions

The inlet boundary conditions are specified the same as in [10]. The computational domain is defined as follows. The origin is at the center of the jet at the inlet plane. The rectangular domain extends in the axial direction to $X_{MAX} = 0.75$m and in the radial direction to $Y_{MAX} = 0.15$m. The numbers of grid cells are shown in Table 2, which is explained below. The number of particles per cell, N_{PC}, is 25. The Courant number used in the particle pseudo time-marching algorithm is 0.2. Time-averaging is a very useful tool to reduce the statistical fluctuations in the FV and particle fields without increasing the number of particles [10]. Both the FV and particle fields are time-averaged. Time-averaged means are defined in the same way as in [10]. The time-averaging factors used are 200 for the particle fields, 20 for the FV fields and 5 for the turbulence fluxes providing to the FV part from the particle part. Artificial viscosity coefficients in the FV algorithm are 0.25 for the 2nd order term and 2.0 for the 4th order term. The ISAT error tolerance is 10^{-4}, which guarantees a 1% tabulation error for temperature and major species and 10% for minor species.

The ARM2 calculation with ISAT is initialized from the flamelet calculation results to provide a better initial guess and hence accelerate the convergence to the statistically-stationary state.

Grid Convergence

Grid convergence is examined using results of calculations with the simple flamelet model on the grids listed in Table 2. The grids used in this paper are slightly different from those used in [10]. The spatial error in the hybrid algorithm has been extensively studied in [9, 10].
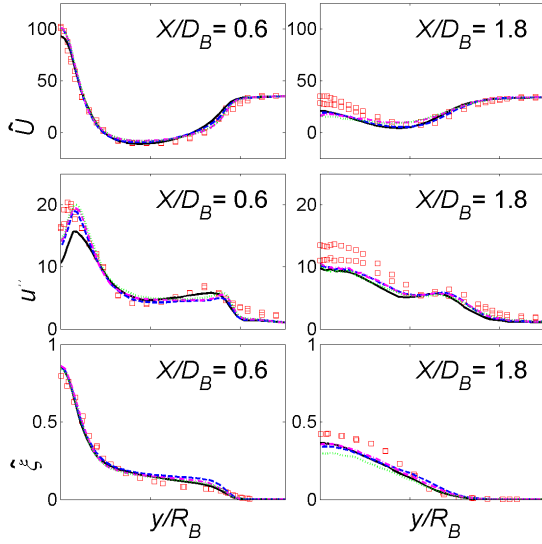
Figure 1: Radial profiles of mean axial velocity (top), r.m.s. of axial velocity (middle), and mean mixture fraction (bottom). Symbols: experimental data, green dotted lines: JPDF-flamelet calculations with Grid 1, magenta dashed-doted lines: JPDF-flamelet calculations with Grid 2, blue dashed lines: JPDF-flamelet with Grid 3, black solid lines: JPDF-flamelet with Grid 4. R_B is the radius of bluff-body.

Therefore an extensive study of spatial error is not repeated here; rather, our goal is simply to show grid convergence of the present results. Figure 1 shows radial profiles of the mean axial velocity, $\tilde{U}$, the r.m.s. of axial velocity, u'', and mean mixture fraction, $\tilde{\xi}$. Two locations, $x/D_B = 0.6$ and $x/D_B = 1.8$ are selected on four grid arrangements, Grid 1, Grid 2, Grid 3, and Grid 4. Figure 1 shows that the three finer grids, Grid 1, Grid 2 and Grid 3 only produce minor variations at most locations for most of fields. The coarsest grid, *i.e.* Grid 4, produces obvious discrepancies, especially for the variance of radial velocity near the first shear layer between the jet and the recirculation zone and the second shear layer between the recirculation zone and the co-flow. Overall, it can be seen that grid convergence is achieved. Grid 3 is used for all subsequent calculations.

Table 2: Grids used to study grid convergence

	Grid 1	Grid 2	Grid 3	Grid 4	SGrid 1
N_X^*	180	144	108	72	72
N_Y^*	160	128	96	64	96

  * N_X and N_Y are the number of cells in the axial and radial directions, respectively.

To reduce computational costs, the detailed chemistry calculations with ISAT use a shorter domain, with $X_{MAX} = 0.36$m. The grid for this domain, SGrid 1, corresponds to a truncated Grid 3. The effects of truncating the computational domain are found to be negligible, especially in the region of our primary interest, say $x/D_B \leq 4.4$, for which the experimental data are available. There are minor discrepancies at downstream locations near the outflow boundary, which are not unexpected because of the effects of the numerical boundary conditions employed at the outflow boundary.

Results and Discussion

In this section, results of JPDF-ISAT calculations of flame HM1 are compared to the experimental data of [1]. As described above, the JPDF model consists of SLM, JPM, IEM, and ARM2 (implemented via ISAT). The IEM mixing model constant C_ϕ is varied from 1.5 to 4.0 to investigate its influence on the prediction of turbulence-finite rate chemical reaction interactions. The results are presented at three axial locations $x/D_B = 0.6$, 1.3 and 1.8. The first location is within recirculation zone. The second location is near the end of recirculation zone. The last location is within the neck zone.

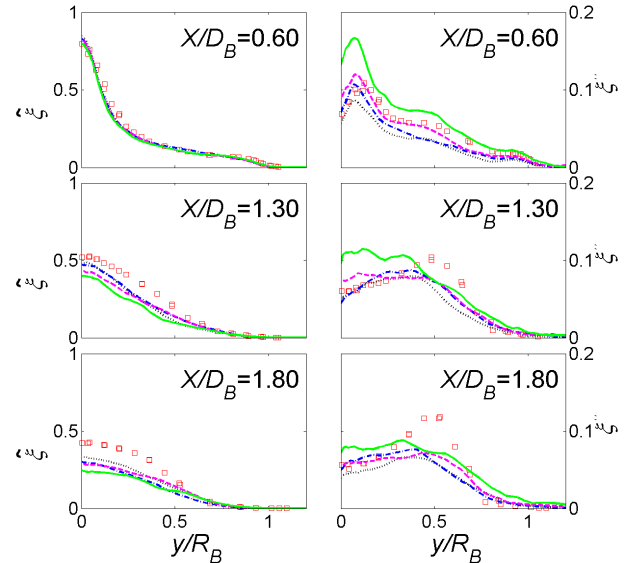Figure 2 shows radial profiles of mean and r.m.s. fluctuations of mixture fraction. The effects of model

Figure 2: Radial profiles of mean and r.m.s fluctuations of mixture fraction. Symbols: experimental data, green solid lines: JPDF-ARM2 calculations with $C_\phi = 1.5$, magenta dashed lines: JPDF-ARM2 calculations with $C_\phi = 2.0$, blue dashed-doted lines: JPDF-ARM2 calculations with $C_\phi = 3.0$, black dotted lines: JPDF-ARM2 calculations with $C_\phi = 4.0$, R_B is the radius of bluff-body.
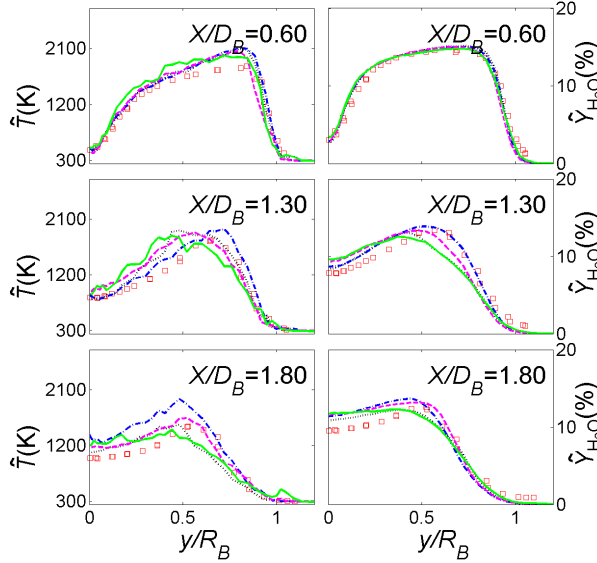
Figure 3: Radial profiles of mean temperature and mean water mass fraction. Symbols: experimental data, green solid lines: JPDF-ARM2 calculations with $C_\phi = 1.5$, magenta dashed lines: JPDF-ARM2 calculations with $C_\phi = 2.0$, blue dashed-doted lines: JPDF-ARM2 calculations with $C_\phi = 3.0$, black dotted lines: JPDF-ARM2 calculations with $C_\phi = 4.0$.
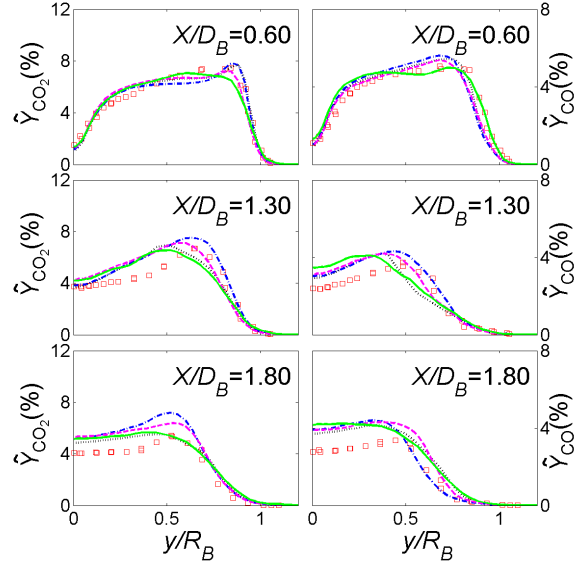

Figure 4: Radial profiles of mean mass fraction of CO_2 and CO. Symbols: experimental data, green solid lines: JPDF-ARM2 calculations with $C_\phi = 1.5$, magenta dashed lines: JPDF-ARM2 calculations with $C_\phi = 2.0$, blue dashed-doted lines: JPDF-ARM2 calculations with $C_\phi = 3.0$, black dotted lines: JPDF-ARM2 calculations with $C_\phi = 4.0$.

constant C_ϕ are also shown. The direct effect of increasing C_ϕ from 1.5 to 4.0 is to increase the mixing and hence to decrease the r.m.s. fluctuation of mixture fraction. It can be clearly seen that the lowest value of C_ϕ (*i.e.*, 1.5) leads to the largest values of r.m.s fluctuation of mixture fraction. Increasing C_ϕ also decreases the scalar flux and consequently decreases the spreading of the mean mixture fraction. This is consistent with the observation in [7].

Generally, the agreement between the JPDF-ARM2 calculation results and the experimental data is reasonably good. The agreement deteriorates somewhat downstream at $X/D_B = 1.8$, where the peak value of the r.m.s. fluctuation of mixture fraction is lower than the experimental data, and the position of the peak value is not captured. Also the values of mean mixture fraction near the center line are under-predicted.

Figure 3 shows the radial profiles of mean temperature and mean H_2O mass fraction. The profiles of temperature are not as smooth as the profiles of the species because the mean temperature is not time-averaged for as long as the other particle properties. In general there is very good agreement between the calculated results and the experimental data, both in profile shape and for peak values of mean temperature and mean H_2O mass fraction. Consistent with the mean mixture fraction profiles, the mean values of temperature and H_2O mass fraction are

over-predicted at downstream locations near the center line.

Radial profiles are plotted in Figure 4 of the mean mass fraction of the carbon species CO_2 and CO. The calculated levels of CO_2 mass fraction are in excellent agreement with experimental data in the recirculation zone. Although the CO mass fraction is slightly over-predicted near the center line, especially downstream, the profiles of mean CO mass fraction are in reasonably good agreement with experimental data within the recirculation zone. The mass fraction of both carbon species are somewhat over predicted near the center line in the neck zone, *e.g.* $X/D_B = 1.8$.

The prediction of carbon species, CO_2 and CO, is improved in the current calculations, relative to the earlier results of Liu *et al* [11], which used the same velocity model, turbulence frequency model and mixing model. The only significant difference in the models is the chemistry mechanism: a C_1 skeletal mechanism was used in the previous calculations. This comparison suggests that ARM removes at least some of the deficiencies of the skeletal mechanism by including important C_2 species. This observation was also made in [7, 17].

Radial profiles of mean mass fraction of the minor species OH and NO are plotted in Figure 5. For the OH radical, the positions of peak values are captured by most of the calculations using various values of the IEM mixing model constant, C_ϕ. At the same time, there is
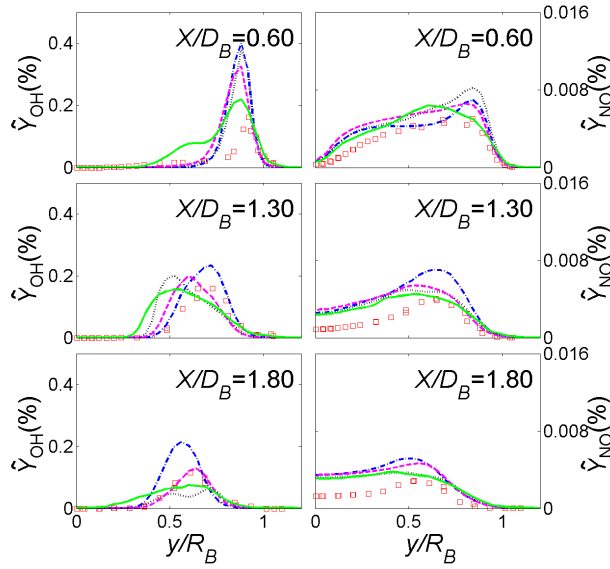
Figure 5: Radial profiles of mean mass fraction of minor species, OH and NO. Symbols: experimental data, green solid lines: JPDF-ARM2 calculations with $C_\phi = 1.5$, magenta dashed lines: JPDF-ARM2 calculations with $C_\phi = 2.0$, blue dashed-doted lines: JPDF-ARM2 calculations with $C_\phi = 3.0$, black dotted lines: JPDF-ARM2 calculations with $C_\phi = 4.0$.

Figure 6: Scatter plots of Temperature against mixture fraction, ξ. The black solid line is laminar flamelet with strained rate $a = 100s^{-1}$, Left: experimental data, right: JPDF calculations. The color represents the radial location of the sample points, ranged between $[0, 1.2R_B]$.

good agreement between the calculations and measurements in profile shape. But the calculated results over-predict the peak values within the recirculation zone, which may be due to our neglect of radiative heat transfer [4]. Better agreement with experimental data is recovered at the downstream locations.

It is seen that the level of OH increases significantly with increasing C_ϕ (Except for the calculations with $C_\phi = 4.0$ at downstream.) The explanation is as follows. The OH radical can be regarded as a reaction indicator, because there is a super-equilibrium amount of OH in the reaction zone in this flame [18]. The super-equilibrium level of OH is mainly determined by the turbulence mixing time scale in the reaction region [19]. Increasing C_ϕ decreases the turbulence mixing time scale, which then increases the level of OH dramatically.

The JPDF predictions of NO with ARM2 are in good agreement with experimental data, although the mean NO mass faction is slightly over-predicted at downstream locations, probably due to the over-prediction of temperature there. The mean NO mass fraction is not very sensitive to the value of C_ϕ.

Figures 6 and 7 show scatter plots of temperature and NO mass fraction against mixture fraction at three axial locations. The calculations are performed with $C_\phi = 2.0$. The JPDF calculated results and experimental data are shown next to each other. The values corresponding to a
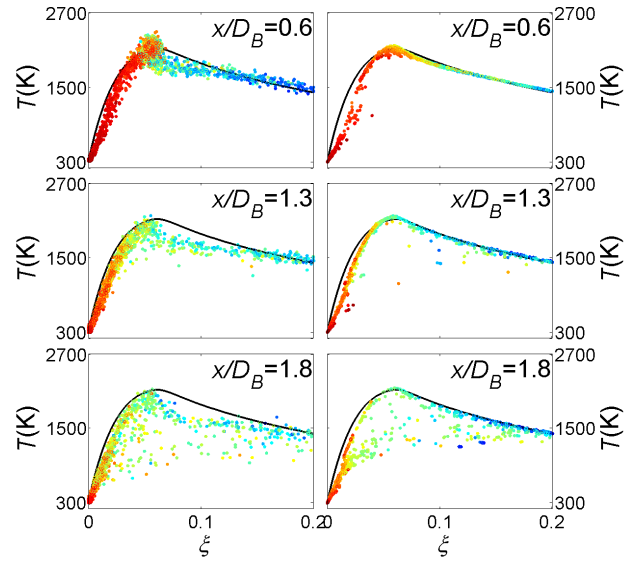
strained ($a = 100\ s^{-1}$) laminar flame is shown for reference. Since all the data at each axial location are plotted together, different colors, (from dark blue to red, corresponding to radial locations $y = 0$ to $1.2R_B$) are used to identify the radial locations. Further investigation is needed to understand the statistical behavior changing with radial location. In the current plots, it is observed that the calculation points are distributed in a narrower band compared with those of the experimental data, especially on the fuel-rich side. This may be due to the deficiencies of the IEM mixing model. The NO mass fraction also is over-predicted on the fuel rich side.

Nevertheless, there is generally good agreement between the results of the calculations and experiments. In particular, the local extinction, which obviously occurs at $X/D_B = 1.8$, as is indicated by sample points with depressed temperature and NO mass fractions, is accurately captured by the JPDF calculations. The banded shape phenomenon in NO mass fraction plots is also observed in [20]. This may be partly due to the features of mixing model and partly due to the ARM2 mechanism.

Conclusions

In this work, a JPDF method implemented as a fully-consistent hybrid FV/Monte Carlo particle algorithm is used to calculate a Sydney bluff-body stabilized flame, HM1. The results presented here demonstrate that the JPDF method using ARM2 mechanism has the capability
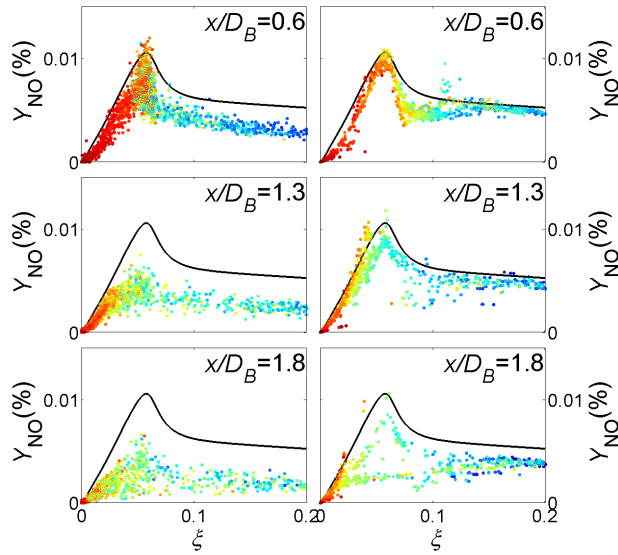
Figure 7: Scatter plots of NO mass fraction against mixture fraction, ξ. The black solid line is laminar flamelet with strained rate $a = 100s^{-1}$, Left: experimental data, right: JPDF calculations. The color represents the radial location of the sample points, ranged between $[0, 1.2R_B]$.

for representing the intense interaction between turbulence and finite-rate chemistry in complex flames such as bluff-body stabilized flames.

1. Stabilized flames are obtained by initializing ISAT-ARM2 calculations from previous simple flamelet calculation results. The calculated mean and variance of mixture fraction, mean of temperature, and mean species mass fraction are generally in good agreement with experimental data. The ARM2 mechanism improves the predictions of CO and NO.

2. The sensitivity of the calculations to the model constant C_ϕ in the IEM mixing model is investigated. Increasing C_ϕ yields higher levels of the radical OH. Generally, the standard value $C_\phi = 2.0$ tends to produce better agreement with the experiments, which is in contrast to the observation in [7].

3. The ISAT algorithm makes it possible to incorporate detailed chemistry in JPDF calculations at a manageable computational cost. Nevertheless, about 90% of the total CPU time is spent on the chemistry calculations. Improvements in the computational efficiency are desirable so that the calculations can be done using more advanced mixing models (such as EMST) which require a larger numbers of particles per cell. It is hoped that the local extinction and reignition in flames HM2 and HM3 can be investigated using the EMST model.

References
1. Masri, A. R., http://www.mech.usyd.edu.au/research/energy/#data/
2. Dally, B. B., Fletcher, D. F., and Masri, A. R., *Combust. Theory Modeling* 2:193-219(1998)
3. Merci, B., Dick, E., Vierendeels, J., Roekaerts, D., and Peeters, T. W. J., *Comb. Flame* 126:1533-1556(2001).
4. Hossain, M., Jones, J. C., and Malalasekera, W., *Flow, Turbulence Combust.* 67:217-234(2001).
5. Kim, S. H. and Huh, K. Y., *Comb. Flame* 130:94-111(2002).
6. Pope, S. B., *Prog. Energy Combust. Sci.* 11:119-192 (1985).
7. Xu, J., and Pope, S. B., *Comb. Flame* 126:94-111(2000).
8. Pope, S. B., *Combust. Theory Modeling*, 1:41-63 (1997).
9. Muradoglu, M., Pope, S. B., and Caughey, D. A., *J. Comput. Phys.* 172:841-878 (2001).
10. Muradoglu, M., Liu, K., and Pope, S. B., *Combust. Flame,* in press.
11. Liu, K., Muradoglu, M., Pope, S. B., and Caughey, D. A., *TNF6,* (2002)
12. Sung, C. J., Law, C. K., and Chen, J.-Y., *Comb. Flame* 125:906-919(2001).
13. Jenny, P., Muradoglu, M., Liu, K., Pope, S. B., Caughey, D. A., *J. Comput. Phys.* 169:1-23 (2001).
14. Muradoglu, M., Pope, S. B., and Caughey, D. A., *Proc. 2nd Joint meeting of US Combust. Inst.* Paper 188 (2001), also to be published in *AIAA J.*
15. Van Slooten, P. R., Jayesh, and Pope, S. B., *Phys. Fluids* 10:246-265 (1998).
16. Dopazo, C., *Phys. Fluids* 18(4):397-404 (1975).
17. James, S. Anand, M. S., Razdan, M. K., and Pope, S. B., *Proc. ASME Turbo. Expo. Land Sea and Air '99,* (1999).
18. Dally, B. B., Masri, A. R., Barlow, R. S., and Fiechtner, G. J., *Comb. Flame* 114:119-148 (1998).
19. Barlow, R. S., Dibble, R. W., Lucht, R. P., and Chen, J.-Y., *Comb. Flame* 82:235-251 (1990).
20. Tang, Q., Xu, J., and Pope, S. B., *Proc. Comb. Inst.* 28:133-139 (2000).